Chapter 13
Fatigue and Creep

In Chap. 12 we described the monotonic behavior of a composite under ambient temperature conditions of loading. There are many applications of composites where cyclic fatigue and high-temperature, i.e., creep conditions prevail. Accordingly, in this chapter we go further in complexity and describe the fatigue and creep behavior of composites. *Fatigue* is the phenomenon of mechanical property degradation leading to failure of a material or a component under cyclic loading. The operative word in this definition is *cyclic*. This definition thus excludes the so-called phenomenon of static fatigue, which is sometimes used to describe stress corrosion cracking in glasses and ceramics in the presence of moisture. Creep refers to time-dependent deformation in a material, which becomes important at relatively high temperatures ($T > 0.4T_m$, where T_m is the melting point in kelvin). We first describe fatigue and then creep of composites.

13.1 Fatigue

Degradation of mechanical properties of a material or a component under cyclic loading is called fatigue. Understanding the fatigue behavior of composites of all kinds is of vital importance, because without such an understanding it would be virtually impossible to gain acceptance of the design engineers. Many high volume applications of composite materials involve cyclic loading situations, e.g., components used in automobile, truck, and mass transit. It would be a fair admission that this understanding of the fatigue behavior of composites has lagged that of other aspects such as the elastic stiffness or strength. The major difficulty in this regard is that the application of conventional approaches to fatigue of composites, for example, the stress vs. cycles (*S–N*) curves or the application of linear elastic fracture mechanics (LEFM), is not straightforward. The main reasons for this are the inherent heterogeneity and anisotropic nature of the composites. These characteristics result in damage mechanisms in composites being very different from those encountered in conventional, homogeneous, or monolithic materials. The fracture behavior of

K.K. Chawla, *Composite Materials: Science and Engineering*,
DOI 10.1007/978-0-387-74365-3_13,

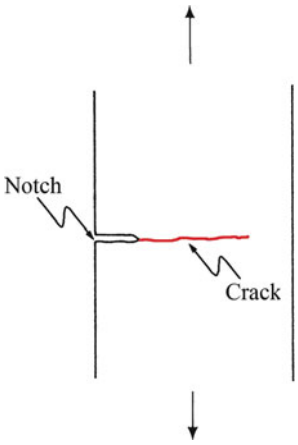

Fig. 13.1 Damage zone in a conventional, homogeneous, monolithic material (isotropic)

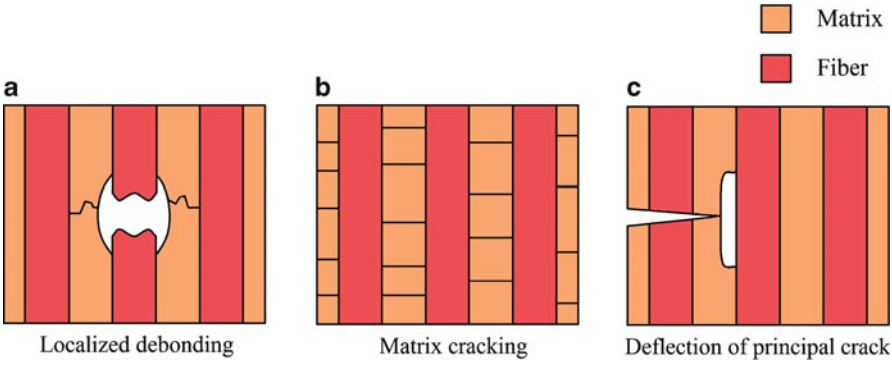

Fig. 13.2 Diffuse damage zone in a fiber reinforced composite (anisotropic): (**a**) fiber break and local debonding; (**b**) matrix cracking; (**c**) deflection of the principal crack along a weak fiber/matrix interface

composites is characterized by a multiplicity of damage modes, such as matrix crazing (in a polymeric matrix), matrix cracking (in a brittle matrix), matrix plasticity (in a ductile matrix), fiber fracture, interfacial debonding and delamination, void growth, and multidirectional cracking, and these modes appear rather early in the fatigue life of composites. The early onset of these different fracture modes leads to progressive loss of stiffness during fatigue of a composite, which is very different from the fatigue behavior of monolithic materials. The different types of damage zones formed in a conventional, isotropic material (e.g., a metal, or ceramic, or polymer) and a fiber reinforced composite, which is an anisotropic material, are shown schematically in Figs. 13.1 and 13.2, respectively. In the case of the isotropic material, a single crack propagates in a direction perpendicular to the cyclic loading

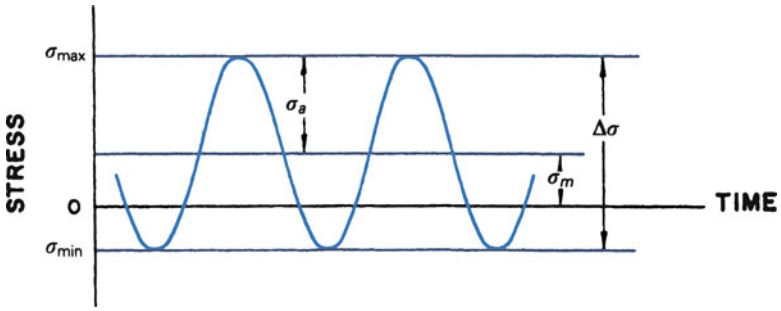

Fig. 13.3 Some useful parameters for fatigue

axis (mode I loading). In the fiber reinforced composite, on the other hand, a variety of subcritical damage mechanisms lead to a highly diffuse damage zone. Despite these limitations, conventional approaches have been used and are therefore described here briefly before we describe some more innovative approaches to the problem of fatigue in composites.

Let us first define some useful parameters for our discussion of the fatigue phenomenon; see Fig. 13.3:

$$\begin{aligned}
&\text{cyclic stress range}, \Delta\sigma = \sigma_{\max} - \sigma_{\min},\\
&\text{cyclic stress amplitude}, \sigma_{\mathrm{a}} = (\sigma_{\max} - \sigma_{\min})/2,\\
&\text{mean stress}, \ \sigma_{\mathrm{m}} = (\sigma_{\max} + \sigma_{\min})/2,\\
&\text{stress ratio}, R = \sigma_{\min}/\sigma_{\max}.
\end{aligned}$$

13.1.1 S–N Curves

We saw in Chap. 10 that in a unidirectionally reinforced fiber composite, elastic modulus and strength improve in the direction of reinforcement. This also has its consequences in the fatigue behavior. *S–N* curves are commonly used with monolithic materials, especially metals and, to some extent, with polymers. It involves determination of the so-called *S–N* curves, where S (or σ_{a}) is the stress amplitude and N is the number of cycles to failure. In general, for ferrous metals, one obtains a fatigue limit or endurance limit. For stress levels below this endurance limit, theoretically, the material can be cycled infinitely. In cases where such an endurance limit does not exist, one can arbitrarily define a cutoff value, a certain number of cycles, say 10^6. Incorporation of fibers generally improves the fatigue resistance of any fiber reinforced composite in the fiber direction. Not surprisingly, therefore, composites containing fibers, aligned along the stress axis and in large volume fractions, do show high monotonic strength values that are translated into high fatigue strength values. Quite frequently, a rule-of-thumb approach in conventional

materials is to increase its monotonic strength, which concomitantly results in an increase in its cyclic strength. This rule-of-thumb assumes that the ratio of fatigue strength/tensile strength is about constant. It should also be noted that the maximum efficiency in terms of stiffness and strength gains in fiber reinforced composites occurs when the fibers are continuous, uniaxially aligned and the properties are measured parallel to the fiber direction. As we go off-angle, the strength and stiffness drop sharply. Also, at off-angles, the role of the matrix becomes more important in the deformation and failure processes. One major drawback of this *S–N* approach to fatigue behavior of a material is that no distinction can be made between the crack initiation phase and the crack propagation phase.

The variety of operating mechanisms and the inadequacy of the *S–N* curve approach have been documented by many researchers. Owen et al. (1967, 1969), for example, studied the fatigue behavior of chopped strand mat glass/polyester composite and observed the following sequence of events in the fatigue failure process: (1) debonding, generally at fibers oriented transverse to the stress axis, (2) cracking in the matrix, and (3) final separation or fracture. The debonding and cracking phenomena set in quite early in the fatigue life. Lavengood and Gulbransen (1969) investigated the importance of fiber aspect ratio and the role of matrix in the fatigue performance of composites. They studied the effect of cyclic loading on short boron fibers (50–55 % volume fraction) in an epoxy matrix. They used a low frequency (3 Hz) to minimize the hysteretic heating effects and measured the number of cycles required to produce a 20 % decrease in the composite elastic modulus, i.e., this was their arbitrary definition of fatigue life. The fatigue life increased with aspect ratio up to about 200, beyond which there was little effect. In all cases, the failure consisted of a combination of interfacial fracture and brittle failure of matrix at 45° to the fiber axis. Incorporation of fibers certainly improves the fatigue resistance of the fiber reinforced polymeric matrix composites in the fiber direction. Not surprisingly, therefore, composites containing these fibers, aligned along the stress axis and in large volume fractions, will show high monotonic strength values, which are translated into high fatigue strength values. An example of *S–N* curves of unreinforced polysulfone (PSF) and composites with a PSF matrix and different amount of short fibers (glass and carbon) is shown in Fig. 13.4a. These results were obtained from tests done at room temperature, cycling frequency between 5 and 20 Hz, and at $R = 0.1$ (Mandell et al. 1983). Izuka et al. (1986) studied the fatigue behavior of two different types of carbon fibers (T800 and T300 carbon fiber) in an epoxy matrix. Both had 60 % fiber volume fraction (V_f) but T800 carbon fiber has a maximum strength of 4.5 GPa and a Young's modulus of 230 GPa while T300 carbon fiber has 3.5 and 210 GPa, respectively. As expected, the higher monotonic strength of T800 carbon fiber resulted in a superior *S–N* curve for the composite.

The polymeric matrices, however, show a viscoelastic behavior and are, generally, poor conductors of heat. Owing to the viscoelastic nature of the polymer matrix, there will be a phase lag between the stress and the strain, i.e., the strain lags the stress or vice versa, and that energy is stored in the material in the form of heat in each cycle. Because of the low thermal conductivity of the polymeric matrix, the heat generated is

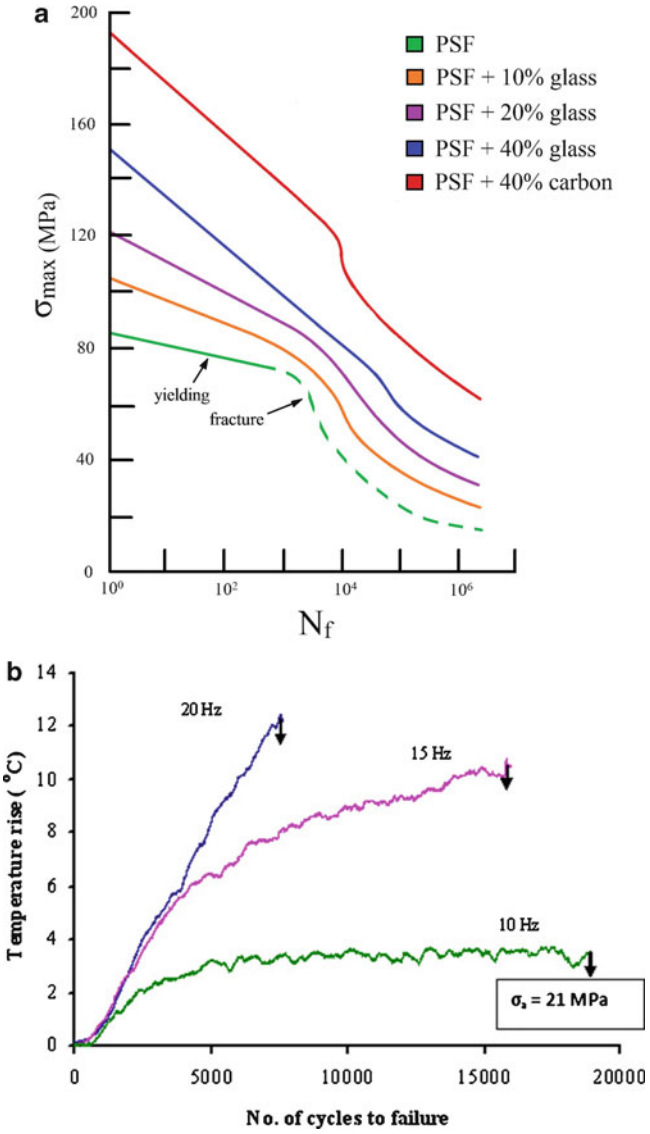

Fig. 13.4 (**a**) *S–N* curves of unreinforced polysulfone (PSF) and composites with a PSF matrix and different amount of short fibers (glass and carbon) [after Mandell et al. (1983)]. (**b**) Temperature rise under fatigue for glass fiber/polypropylene composites (Goel et al. 2009). At a given stress amplitude, temperature rises more quickly at higher frequency and leads to premature failure of the composite

not dissipated quickly. This can cause a temperature difference between the interior and the surface of a PMC, and the fatigue behavior of PMCs becomes even more complex due to such internal heating. The internal heating phenomenon, of course, depends on the cycling frequency. For a given stress level, this temperature difference

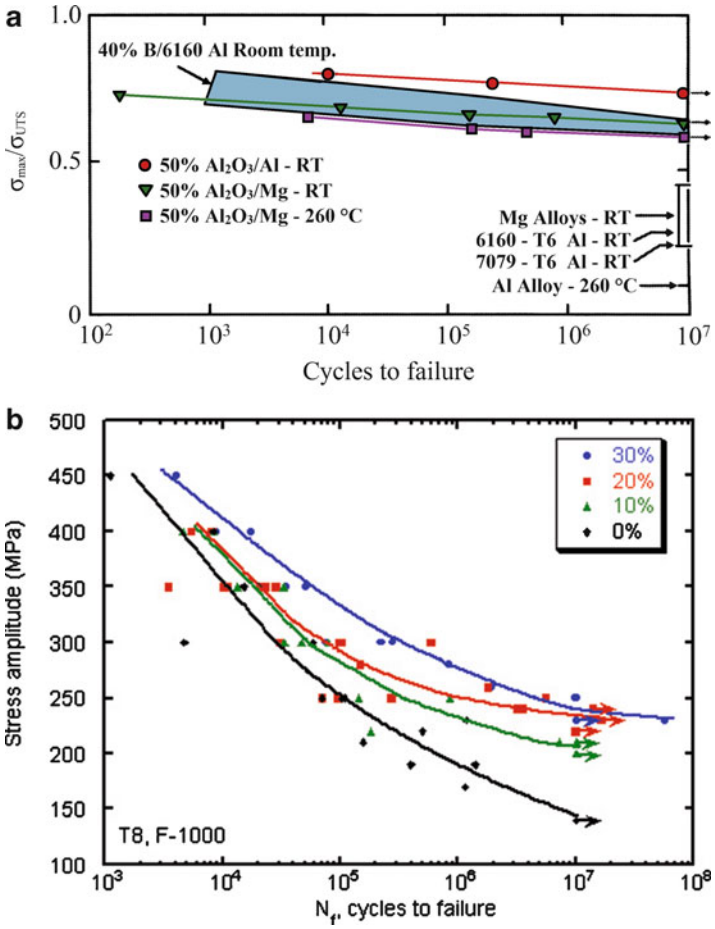

Fig. 13.5 (**a**) *S–N* curves for MMCs in tension–tension for unidirectionally reinforced boron fiber (40 % v/o)/A16061, alumina fiber (50 % v/o)/Al, and alumina fiber (50 % v/o)/Mg composites [after Champion et al. (1978)]. (**b**) *S–N* curves for silicon carbide particle reinforced aluminum matrix composites [courtesy of N. Chawla]

increases with increasing frequency. Figure 13.4b shows this for glass fiber/polypropylene composites (Goel et al. 2009). At a given stress amplitude, temperature rises more quickly at higher frequency and leads to premature failure of the composite.

Typically, the carbon fibers are much more effective in improving the fatigue behavior of a given polymeric matrix than glass fibers. The reasons for this are the high stiffness and high thermal conductivity of carbon fibers vis-à-vis glass fibers. The higher thermal conductivity of carbon fibers will contribute to a lower hysteretic heating of the matrix at a given frequency.

Examples of *S–N* curves for fiber reinforced MMCs are shown in Fig. 13.5a, which shows the *S–N* curves in tension–tension for unidirectionally reinforced

boron (40 % v/o)/A16061, alumina (50 % v/o)/Al, and alumina (50 % v/o)/Mg composites (Champion et al. 1978). The cyclic stress is normalized with respect to the monotonic ultimate tensile stress. Note the rather flat *S–N* curves in all the cases and the fact that the unidirectional composites show better fatigue properties than the matrix when loaded parallel to the fibers. For example, at 10^7 cycles, the fatigue-to-tensile strength ratio of the composite is about 0.77, almost double that of the matrix. *S–N* curves for silicon carbide particle reinforced aluminum matrix composites are shown in Fig. 13.5b. Increase in volume fraction of SiC_p results in an increase in fatigue life (Chawla et al. 1998a, b).

Gouda et al. (1981) observed crack initiation early in the fatigue life at defects in boron fibers in unidirectionally reinforced B/Al composites. These cracks then grew along the fiber/matrix interface and accounted for a major portion of the fatigue life, as would be the case in a composite with a high fiber-to-matrix strength ratio. In composites with low fiber-to-matrix strength ratios, crack propagation may take up a major portion of fatigue life, but the crack would be expected to grow across the fibers and a poor fatigue resistance will result. This simply confirms the observation that in unidirectional composites the fatigue resistance will be maximum along the fiber direction and the greatest efficiency will be achieved if the fibers have uniform properties, as much as possible defect-free, and much stronger than the matrix. Similar results have been obtained by other researchers. For example, McGuire and Harris (1974) studied the fatigue behavior of tungsten fiber reinforced aluminum–4 % copper alloy under tension–compression cycling $(R = \sigma_{min}/\sigma_{max} = -1)$. They found that increasing the fiber volume fraction from 0 to 24 % resulted in increased fatigue resistance. This was a direct result of increased monotonic strength of the composite as a function of the fiber volume fraction. The reader should note that due to the highly anisotropic nature of the fiber reinforced composites in general, the fatigue strength of any off-axis fibrous composite will be expected to decrease with increasing angle between the fiber axis and the stress axis. This has been confirmed by studies involving *S–N* behavior of alumina fiber reinforced magnesium composites (Hack et al. 1987; Page et al. 1987) It was found that the *S–N* behavior followed the tensile behavior. Increased fiber volume fractions resulted in enhanced fatigue life times in the axial direction but little or no improvement was observed in the off-axis directions. Fatigue crack initiation and propagation occurred primarily through the magnesium matrix. Thus, alloy additions to increase the strength of the matrix and fiber/matrix interface were tried. The alloy additions did improve the off-axis properties but decreased the axial properties. The reason for this was that while the alloy additions resulted in the matrix and interface strengthening, they decreased the fiber strength. Similar effect of fiber orientation on fatigue properties exists in PMCs. As an example, Goel et al. (2009) observed better fatigue performance in the longitudinal direction than in the transverse direction in glass fiber/polypropylene composites.

13.1.2 Fatigue Crack Propagation

Fatigue crack propagation tests are generally conducted in an electro-hydraulic closed-loop testing machine on notched samples. The results are presented as log da/dN (crack growth per cycle) vs. log ΔK (cyclic stress intensity factor). Crack growth rate, da/dN, is related to the cyclic stress intensity factor range, ΔK, according to the power law relationship formulated by Paris and Erdogan (1963):

$$\mathrm{d}a/\mathrm{d}N = A(\Delta K)^{\mathrm{m}}, \tag{13.1}$$

where A and m are constants that depend on the material and test conditions. The applied cyclic stress intensity range is given by

$$\Delta K = Y\Delta\sigma\sqrt{\pi a},$$

where Y is a geometric factor, $\Delta\sigma$ is the cyclic stress range, and a is the crack length. The major problem in this kind of test is to make sure that there is one and only one dominant crack that is propagating. This is called the *self-similar* crack growth, i.e., the crack propagates in the same plane and direction as the initial crack. Fatigue crack propagation studies, under conditions of self-similar crack propagation, have been made on metallic sheet laminates (McCartney et al. 1967; Taylor and Ryder 1976; Pfeiffer and Alic 1978; Chawla and Liaw 1979; Godefroid and Chawla 1988) and unidirectionally aligned fiber reinforced MMCs (Saff et al. 1988). For the crack arrest geometry, if the interface is weak, then the crack on reaching the interface bifurcates and changes its direction and thus the failure of the composite is delayed. The improved fatigue crack propagation resistance in crack divider geometry has been attributed either to interfacial separation, which relieves the triaxial state of stress, or to an interfacial holding back of crack in the faster crack-propagating component by the slower crack-propagating component. Generally, a relationship of the form of Eq. (13.1) describes the fatigue crack propagation behavior.

In general, the fibers provide a crack-impeding effect but the nature of the fiber (morphology, rigidity, and fracture strain), the fiber/interface, and/or any reaction zone phases that might form at the interface can have great influence.

Fatigue crack propagation studies have also been done on aligned eutectic or in situ composites. Because many of these in situ composites are meant for high-temperature applications such as in turbines, their fatigue behavior has been studied at temperatures ranging from room temperature to 1,100 °C. The general consensus is that the mechanical behavior of in situ composites, static and cyclic strengths, is superior to that of the conventional cast superalloys (Stoloff 1987).

It should be emphasized that only fatigue crack propagation rate data obtained under conditions of self-similar propagation can be used for comparative purposes. In a composite consisting of plies with different fiber orientation, in general, the self similar mode of crack propagation will not be obtained.

13.1.2.1 Fatigue of Composites under Compression

Fiber reinforced composites generally show lower fatigue resistance in compression than in tension. This may be due to the cooperative buckling of adjacent fibers and the accompanying matrix shear. In monotonic compression of unidirectionally reinforced fiber composites, a fiber kinking mechanism leads to failure. The failure in this case initiates at a weak spot, e.g., at a point where the fiber/matrix bonding is weak. This initial failure will, in turn, destabilize the neighboring fibers, causing more kink failure. Eventually, various kink failure sites can coalesce and lead to transverse tensile loading of the composite and longitudinal splitting. Pruitt and Suresh (1992) showed that in addition to kink band formation, in unidirectional carbon fiber/epoxy composites under cyclic compression, a single mode I crack can start and grow perpendicular to the fiber axis. This compression fatigue phenomenon is thought to be macroscopically similar to that observed in metals, polymers, and ceramics. The origin of a mode I crack ahead of a stress concentration is the presence of residual tensile stresses which can result from a variety of permanent damage modes involving matrix, fiber, interface, etc.

One can also introduce defects to simulate a delamination in fiber reinforced laminated composites and then study its propagation under conditions of fatigue. Such defects may be introduced in a laminate by one of the following means:

1. Insert circular inserts of different diameters at different interfaces
2. Insert a hole in the laminate
3. Produce defects in a laminate by controlled, low-velocity impacts

Delamination growth under cyclic compression fatigue in a 38-ply T300 carbon/5208 epoxy composite laminate was studied by O'Brien (1984). The maximum strain decreased with cycling. The impacted laminates suffered the most severe degradation on compressive cycling, while the laminates with a single implanted delamination suffered the least damage.

13.1.2.2 Fatigue Behavior of CMCs

We describe the fatigue behavior of CMCs under a separate subheading because of new discoveries. Conventional wisdom had it that cyclic fatigue was unimportant so far as ceramics were concerned. However, in actuality the subject of cyclic fatigue in ceramics and ceramic matrix composites *is* an important one. Engineers and researchers began to appreciate the importance of cyclic fatigue in ceramics and ceramic matrix composites only in the 1970s. The fracture resistance of CMCs under cyclic conditions needs to be evaluated for design in a variety of potential structural applications. For example, it is not unusual to have a design requirement for a ceramic component in an automotive gas turbine to withstand more than 30,000 cycles of fatigue (low-cycle fatigue) (Helms and Haley 1989). In the case of

carbon fiber reinforced glass composites, no significant loss of strength was observed on cyclic loading (Phillips 1983). However, the density and penetration of matrix cracks was more under cyclic loading than under static loading conditions. Also, under static loading this CMC showed higher work of fracture than under cyclic loading. Prewo et al. (1986) studied the tensile fatigue behavior of Nicalon-type silicon carbide fiber reinforced lithium aluminosilicate (LAS) glass–ceramic composite. They used two different types of LAS as the matrix material: one showed a linear tensile stress–strain curve to failure (LAS I) while the other showed a markedly nonlinear behavior due to extensive matrix cracking prior to ultimate failure (LAS II). It was observed that the level of tensile stress at which the inelastic behavior (proportional limit) of the composite began had an important bearing on the fatigue behavior of the CMC. The residual tensile strength and elastic modulus of the LAS I composite after fatigue was the same as that of as-fabricated composite. In the LAS II composite, cycling below the proportional limit produced the same result. However, on cycling to stress levels higher than the proportional limit, a second linear stress–strain region having a modulus less than the initial modulus was observed. Presumably, this change in behavior was due to matrix microcracking at stresses above the proportional limit.

It was generally thought that the phenomenon of cyclic fatigue was unimportant in ceramics. Work by Suresh and coworkers (Suresh et al. 1988; Suresh 1991; Han and Suresh 1989) on fatigue crack growth in a variety of brittle solids in compression, tension, and tension-compression fatigue shows that mechanical fatigue effects, i.e., due to cyclic loading, occur at room temperature in brittle solids as well. A variety of mechanisms such as microcracking, dislocation plasticity, stress- or strain-induced phase transformations, interfacial slip, and creep cavitation can promote an inelastic constitutive response in brittle solids of all kinds under compressive cycling. Particularly, in CMCs, the mechanisms of crack-tip deformation differ significantly under static and cyclic loading. They demonstrated that under pulsating compression, nucleation and growth of stable fatigue cracks occurred even at room temperature. Suresh et al. showed conclusively that cyclic compressive loading caused mode I fatigue crack growth in SiC whiskers/Si_3N_4 matrix composites. They also observed whisker pullout and breakage after fatigue cycling. Such behavior is generally not observed under monotonic loading. This mode I fatigue crack growth under far-field cyclic compression occurs because a residual zone of tensile stress is generated at the crack tip on unloading. Wang et al. (1991) investigated the behavior of a [0/90] carbon fiber reinforced silicon carbide composite under cyclic loading. They used tension–tension loading of smooth and notched samples and compression–-compression loading. Damage in pulsating tension consisted of cumulative microcracking and spalling. In this regard, it worth pointing out that investigation of cyclic behavior of polycrystalline continuous alumina fiber showed a definite cyclic fatigue effect, i.e., cyclic fatigue of alumina fibers showed more damage than static fatigue (Chawla et al. 2005).

An important problem in high-temperature behavior of polycrystalline ceramics is the presence of intergranular glassy phases. Sintering and other processing aids

can form glassy phases at the boundaries, which can result in rather conspicuous subcritical crack growth. Such subcritical crack growth can become very important in ceramic matrix composites because fibers such as silicon carbide can undergo oxidation. Han and Suresh (1989) examined the tensile cyclic fatigue crack growth in a silicon carbide whisker (33 vol.%)/alumina composite at 1,400 °C. The composite showed subcritical fatigue crack growth at stress intensity values far below the fracture toughness. The fatigue behavior was characterized by the cyclic stress intensity factor, stress ratio, and frequency. They examined the crack tip region by optical and transmission electron microscopy and found that the nucleation and growth of flaws at the interface was the main damage mechanism. Diffuse microcracking in the wake of the crack and crack deflection/branching were observed. An increase in the test temperature (or the cyclic stress intensity or a reduction in the loading rate) can cause a rather significant increase in the size of the damage zone at the crack tip. Han and Suresh observed oxidation of silicon carbide whiskers to a silica-type glassy phase in the crack tip region at 1,400 °C, in air. The alumina matrix can react with the main oxidation product, viz., SiO_2, to form aluminosilicates, SiC-rich or stoichiometric mullite, and the like. Viscous flow of glass can result in interfacial debonding, followed by the nucleation, growth, and coalescence of cavities. The important thing to note is that there is a difference in deformation and failure mechanisms under static and cyclic loadings, even in CMCs.

In a manner analogous to PMCs, there can be a hysteretic heating in CMCs under cyclic loading conditions due to interfacial friction (Holmes 1991). Sørensen and Holmes (1995) observed that a lubricating layer may be beneficial in improving fatigue life of CMCs. A thicker coating, which would be expected to provide greater protection to the fiber against abrasion damage, resulted in less frictional heating because of less wear of the fibers during fatigue of a chemical vapor infiltrated (CVI) Nicalon/C/SiC composite (Chawla 1997 and Chawla et al. 1998a, b). The composite with a thinner coating exhibited much higher frictional heating. At higher frequencies, more heating was observed since the energy dissipated per unit time also increased. Substantial damage in terms of loss of stiffness was observed in fatigue of Nicalon/C/SiC, with most of the damage occurring during the first cycle. At a constant stress, the level of damage was not significantly dependent on frequency. At a given frequency, however, higher stresses induced more damage in both composites. In the case of the fiber in the form of a plain-weave fabric, a recovery in modulus of these woven composites was observed due to stretching and alignment of the fabric during fatigue, creating a stiffer reinforcing architecture.

The laminate stacking sequence can affect the high-frequency fatigue behavior of CMCs. In SCS-6/Si_3N_4 composites, frictional heating in angle-ply laminates [±45] was substantially higher than that in cross-ply laminates [0/90] (Chawla 1997). Because the angle ply had a lower stiffness, matrix microcracking in this composite was more predominant. Temperature rise in the specimens correlated very well with stiffness loss as a function of fatigue cycles in the composites (see Sect. 13.1.3).

13.1.2.3 Fatigue of Particle and Whisker Reinforced Composite

Ceramic particle reinforced metal matrix composites, such as silicon carbide or alumina particle reinforced aluminum alloy composites can have improved fatigue properties vis-à-vis unreinforced aluminum alloys, which can make these composites useful in applications where aluminum alloys would not be considered (Allison and Jones 1993). Such systems have been studied by some researchers (Chawla et al. 1998a, b; Crowe and Hasson 1982; Williams and Fine 1985, 1987; Logsdon and Liaw 1986; Shang et al. 1988; Davidson 1989; Kumai et al. 1990; Bonnen et al. 1990; Christman and Suresh 1988a, b). In general, in terms of *S–N* curve behavior, the composite shows an improved fatigue behavior vis-à-vis the unreinforced alloy. Such an improvement in stress-controlled cyclic loading or high cycle cyclic fatigue is attributed to the higher stiffness of the composite. However, the fatigue behavior of the composite, evaluated in terms of strain amplitude vs. cycles or low-cycle fatigue, was inferior to that of the unreinforced alloy (Bonnen et al. 1990). This was attributed to the generally lower ductility of the composite compared to the unreinforced alloy.

Particle or short fibers can provide easy crack initiation sites. The detailed behavior can vary depending on the volume fraction of the reinforcement, shape, size, and most importantly on the reinforcement/matrix bond strength. For example, Williams and Fine (1987) observed fatigue crack initiation at the poles of SiC whiskers in 2124 aluminum. They also observed arrest of short cracks at the whisker/Al interfaces. Frequently in aluminum matrix composites, especially those made by casting, there are particles, called constituent particles in aluminum literature, other than SiC, such as $CuAl_2$, $(Fe,Mn)_3{\cdot}SiAl_{12}$, and $Cu_2Mg_5Si_6Al_5$ (Kumai and Knott 1991). During liquid metal processing of particle reinforced MMCs, there occurs the phenomenon of particle pushing ahead of the solidification front (Rohatgi et al. 1994). This results in SiC particles and the constituent particles decorating the cell boundaries in the aluminum alloy matrix.

Some possible interactions between the ceramic particle reinforcement and the crack tip in the matrix are shown schematically in Fig. 13.6a. When the ceramic particles are large, they can be loaded to the point of fracture and the fatigue crack runs though the particles. When we have fine particles, the crack goes around the particles. Examples of such behavior can be found in practical composites (SiC_p/Al alloy) (Chawla and Ganesh 2010). Figure 13.7 shows schematic representations of crack growth vs. cyclic intensity factor for a monolithic alloy and a particulate composite. Levin et al. (1989) observed superior resistance to fatigue crack growth in 15 vol.% SiC particle/Al 6061 composite vis-à-vis Al 6061 alloy, which was attributed to a slower crack growth rate in the composite due to crack deflection caused by the SiC particles. Computer simulation of crack growth behavior in particle reinforced MMCs starting with actual microstructures rather than simplified models has become quite important. Ceramic particle shape, size

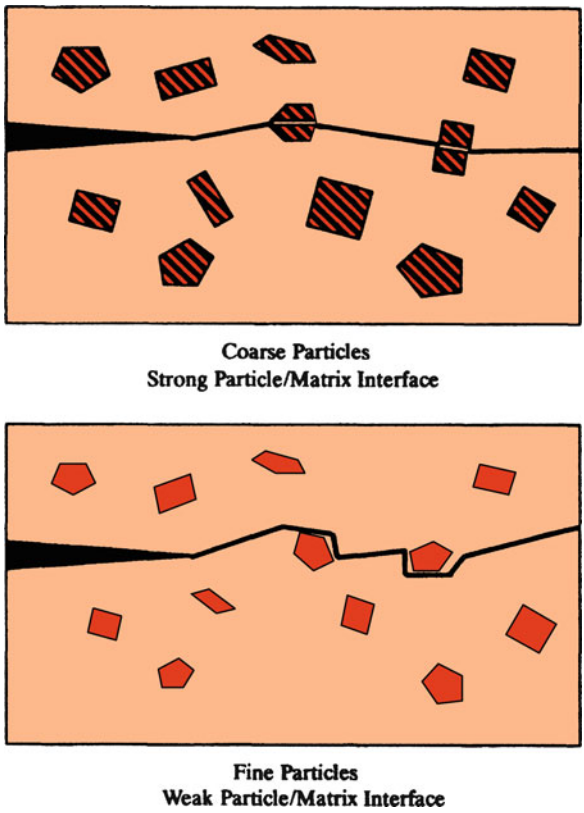

Fig. 13.6 Some possible particle reinforcement and crack tip interactions

distribution, spatial distribution, etc. are very important during deformation of these materials, particularly during crack growth.

It would appear that choosing the optimum particle size and volume fractions, together with a clean matrix alloy, will result in a composite with improved fatigue characteristics. Shang et al. (1988) examined the effect of particle size on fatigue crack propagation as a function of cyclic stress intensity in a silicon carbide particle reinforced aluminum. They observed that for fine particle size, the threshold stress intensity, ΔKth, for the composite was less than that for the unreinforced alloy, i.e., initial fatigue crack growth resistance of the composite was less than that of the unreinforced alloy. For coarse particles, the threshold intensity values were about the same for the two, while at very high values of the cyclic stress intensity, the fatigue crack growth of the composite was less than that of the unreinforced alloy.

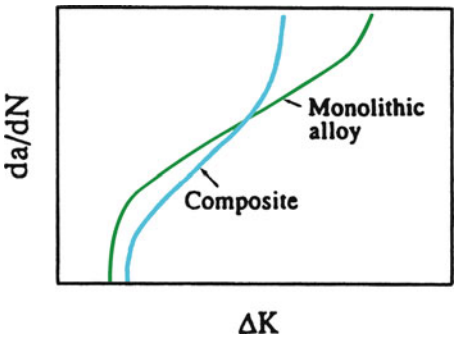

Fig. 13.7 Schematic representation of crack growth vs. cyclic intensity factor for a monolithic alloy and a particulate MMC [after Kumai et al. (1990)]

13.1.3 Damage Mechanics of Fatigue

It was mentioned earlier that the complexities in composites lead to the presence of many modes of damage, such as matrix cracking, fiber fracture, delamination, debonding, void growth, and multidirectional cracking. These modes appear rather early in the fatigue life of composites, i.e., these subcritical damage accumulation mechanisms come into play rather early in the fatigue life—well before the fatigue limit, as determined in an *S*–*N* test, and a highly diffuse damage zone is formed. One manifestation of such damage is the stiffness loss as a function of cycling. In general, one would expect the scatter in fatigue data of composites to be much greater than that in fatigue of monolithic, homogeneous materials. Again, this is because of the existence of a variety of damage mechanisms in composites, to wit, random distribution of matrix microcracks, fiber/matrix interface debonding, and fiber breaks, etc. With continued cycling, an accumulation of damage occurs. This accumulated damage results in a reduction of the overall stiffness of the composite laminate. Measurement of stiffness loss as a function of cycling has been shown to be quite a useful technique for assessing the fatigue damage in composites. Information useful to designers can be obtained from such curves. In MMCs, the fatigue behavior of boron fiber and silicon carbide fiber reinforced aluminum and titanium alloy matrix composite laminates with different stacking sequences has been examined using the stiffness loss measurement technique (Dvorak and Johnson 1980; Johnson 1988; Johnson and Wallis 1986). It was observed that on cycling below the fatigue limit but above a distinct stress range, ΔS_{SD}, the plastic deformation and cracking (internal damage) in the matrix led to a reduced modulus. Figure 13.8 shows the response of a boron fiber/aluminum matrix composite subjected to a constant cyclic stress range (225 MPa) with varying values of S_{max}, the maximum stress. The modulus drop occurred only when S_{max} was shifted upward. Johnson (1988) proposed a model that envisioned that the specimen reached a saturation damage state (SDS) during constant-amplitude fatigue testing. Gomez and Wawner (1988) also observed stiffness loss on subjecting silicon carbide fiber/aluminum composites to tension–tension fatigue ($R = 0.1$) at 10 Hz.

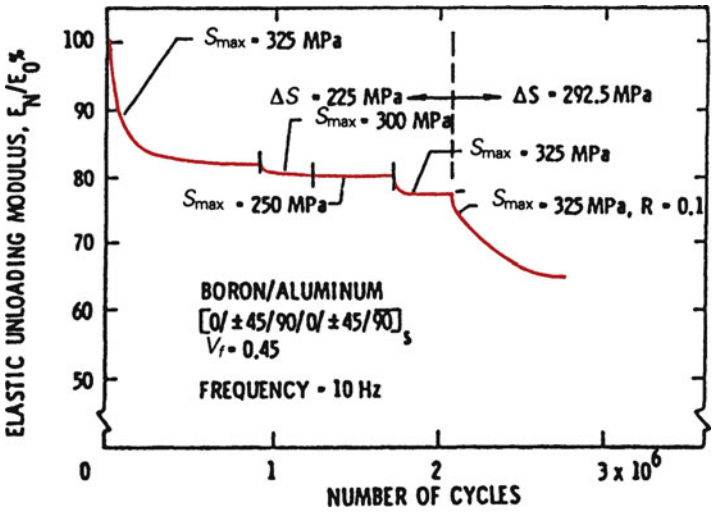

Fig. 13.8 Response of a boron fiber/aluminum matrix composite subjected to a constant cyclic stress range (225 MPa) with varying values of S_{max}, the maximum stress [after Johnson (1988)]

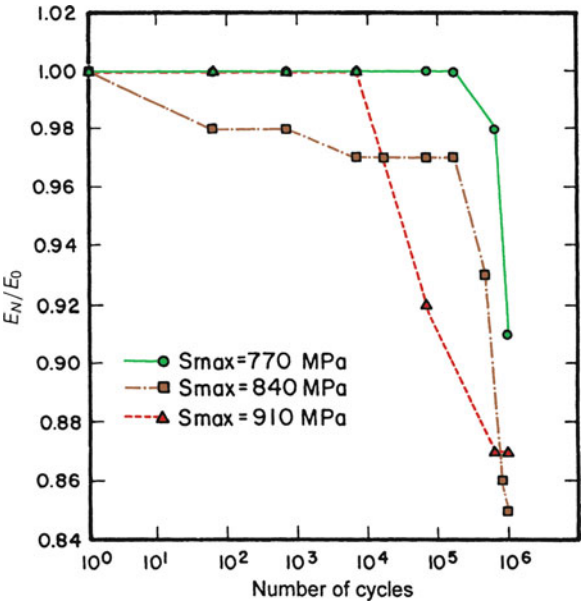

Fig. 13.9 Typical modulus loss curve for unidirectional silicon carbide/aluminum composites. E_N is the modulus after N cycles and E_0 is the modulus in the uncycled state [after Gomez and Wawner (1988)]

Periodically, the cycling was stopped and the elastic modulus was measured. Figure 13.9 shows a typical modulus loss curve for unidirectional silicon carbide fiber/aluminum composites. Modulus at N cycles, E_N, normalized with respect to the original modulus, E_0, is plotted against the log (number of cycles, N). These authors used a special type of silicon carbide fiber, called the SCS-8 silicon carbide fiber, which is a silicon carbide fiber with a modified surface to give a strong bond between the fiber and the aluminum matrix. The SCS coating broke off at high cycles and the fracture surface showed the coating clinging to the matrix. Stiffness loss as a function of number of cycles was also observed for Nicalon fiber/borocilicate glass-ceramic matrix composites (Ramakrishnan and Jayaraman 1993). In CMCs, the matrix can have a lower strain-to-failure than the fibers. In such a case, the matrix starts cracking first. Thereafter, we have two possible routes. In the case of a weak interface, we observe fiber/matrix debonding followed by fiber pullout, etc. In the case of a strong interface, matrix cracking leads to failure and a brittle failure of the composite. Karandikar and Chou (1992) used the approach of stiffness loss as a function of stress cycles with unidirectionally reinforced Nicalon fiber/calcium aluminosilicate (CAS) composites and obtained correlations between crack density and stiffness reduction.

Let us now focus our attention on the fatigue behavior of fiber reinforced *laminated composites* that are made by consolidating prepregs. Figure 13.10a shows schematically a comparison of damage accumulation as a function of fatigue cycles in a laminated composite made by appropriately stacking differently oriented plies and a monolithic, homogeneous material under constant stress amplitude fatigue (Hahn and Lorenzo 1984). We plot damage ratio against cycle ratio. The damage ratio is the current damage normalized with respect to the damage at final failure. The cycle ratio, similarly, is the number of cycles at a given instant divided by the number of cycles to failure. In a conventional, homogeneous material, the term *damage* simply represents the crack length, and not surprisingly it increases monotonically with cycling. In the case of a laminate, we do not have a simple and unambiguous manifestation of damage, such as a crack length. Instead, damage is diffuse and involves a variety of cracks; so damage, in principle, would mean the crack density. Note that, unlike in homogeneous materials, the damage (i.e., crack density) in laminates accelerates at first and then decelerates with cycling. This distinctive behavior is very important. Such a multiplicity of fracture modes is common to all composites. As an example, Figure 13.10b shows the fracture surface of B(W)/A1 6061 composite made by diffusion bonding. Note the ductile fracture in aluminum, brittle fracture in boron, fiber pullout (see the missing fiber in top-left-hand corner), and sheet delamination.

As was pointed out earlier, the fiber reinforced laminates can sustain a variety of subcritical damage (crazing and cracking of matrix, fiber/matrix decohesion, fiber fracture and pullout, ply cracking, delamination, and so on). For example, the cracking of a ply will result in a relaxation of stress in that ply, and with continued cycling no further cracking occurs in that ply. Ply cracking generally involves cracking in the matrix and along the fiber/matrix interface but rarely any fiber fracture. Other damage-accumulating mechanisms include the growth of existing

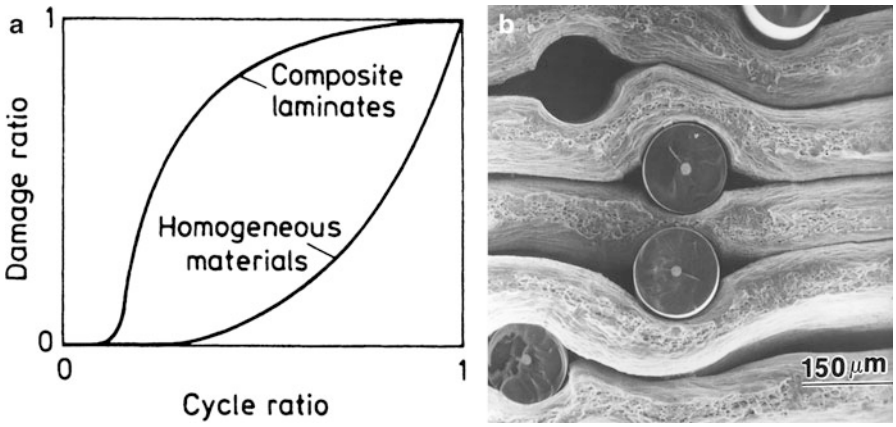

Fig. 13.10 (**a**) Comparison of damage accumulation as a function of fatigue cycles in a laminated composite (made by appropriately stacking differently oriented plies) and a monolithic, homogeneous material under constant stress amplitude fatigue [after Hahn and Lorenzo (1984)]. (**b**) Fracture surface of B(W)/A1 6061 composite made by diffusion bonding. Note the different modes of damage: ductile fracture in aluminum, brittle fracture in boron, fiber pullout (see the missing fiber in *top-left-hand corner*), and sheet delamination

cracks into interfaces leading to ply delamination. The subcritical damage can accumulate rather rapidly on cycling.

The various types of subcritical damage mentioned above result in a reduction of the load-carrying capacity of the composite, which in turn manifests itself as a reduction in stiffness and strength of the composite. Many researchers have experimentally related the stiffness changes in the laminated composites to the accumulated damage under fatigue (Hahn and Kim 1976; Highsmith and Reifsnider 1982; Talreja 1985; Ogin et al. 1985). Work with polymer– and metal–matrix composites shows that this change in stiffness values is a good indicator of the extent of damage in these composites. The various types of subcritical damage mentioned above result in a reduction of the load-carrying capacity of the laminate composite, which in turn manifests itself as a reduction of laminate stiffness and strength (Hahn and Kim 1976; Highsmith and Reifsnider 1982; Talreja 1985; O'Brien and Reifsnider 1981; Ogin et al. 1985). Figure 13.11 depicts schematically the changes in crack density, delamination, and modulus in a composite laminate under fatigue (Hahn and Lorenzo 1984). Reifsnider et al. (1981) modeled the fatigue development in laminate composites as occurring in two stages. In the first stage, homogeneous, noninteractive cracks appear in individual plies. In the second stage, the damage gets localized in zones of increasing crack interaction. The transition from stage one to stage two occurs at what has been called the *characteristic damage state* (CDS), which consists of a well-defined crack pattern characterizing saturation of the noninteractive cracking. Talreja (1985) used this model to determine the probability distribution of the number of cycles required to attain the CDS.

It can safely be said that the change in stiffness values is a good indicator of the damage in composites. An actual stiffness reduction curve for a [0°/90°]s glass fiber reinforced laminated composite is shown in Fig. 13.12 (Ogin et al. 1985). Under cyclic loading of a laminated composite, a variety of damage accumulation mechanisms can start at stress levels below those needed under monotonic conditions. Because of the presence of this multiplicity of failure modes in a fibrous composite, it rarely fails in a simple manner as does a monolithic material. Following Beaumont (1989), we define the failure of the composite when a critical level of damage is reached or exceeded. Let D be the damage parameter that

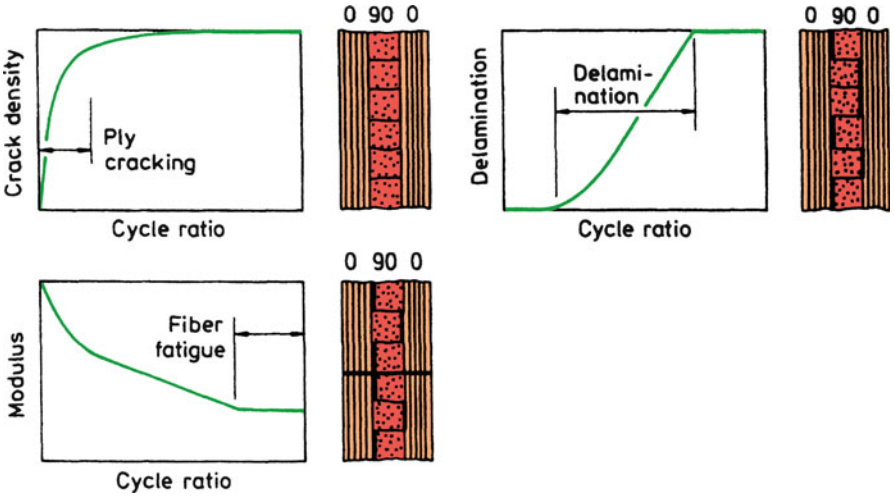

Fig. 13.11 Schematic of changes in crack density, delamination, and modulus in a composite laminate under fatigue [after Hahn and Lorenzo (1984)]

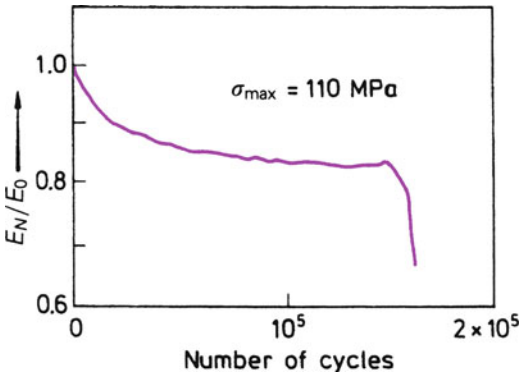

Fig. 13.12 Stiffness reduction curve for a $[0°/90°]_s$ glass fiber reinforced laminated composite [after Ogin et al. (1985)]

increases as a function of number of cycles, N. Then, $\mathrm{d}D/\mathrm{d}N$ will be the damage growth rate. We can write for the damage growth rate

$$\mathrm{d}D/\mathrm{d}N = f(\Delta\sigma, R, D), \tag{13.2}$$

where $\Delta\sigma$ is the cyclic stress range, R is the stress ratio, and D is the current value of damage. Let N_f be the number of cycles to failure, i.e., the fatigue life corresponding to a critical level of damage. Then integrating Eq. (13.2) between limits of initial damage, D_i and final damage, D_f, we can write for the number of cycles to failure as

$$N_\mathrm{f} = \int_{D_\mathrm{i}}^{D_\mathrm{f}} \mathrm{d}D/f(\Delta\sigma, R, D). \tag{13.3}$$

The main problem is that the function f is not known. One measure of damage is the instantaneous load-bearing capacity or the stiffness, E. We can write

$$E = E_0 g(D), \tag{13.4}$$

where E_0 is the stiffness of the undamaged material and $g(D)$ is a function of damage, D.

Rewriting Eq. (13.4) as $E/E_0 = g(D)$ and differentiating, we get

$$(1/E_0)\mathrm{d}E/\mathrm{d}N = \mathrm{d}g(D)/\mathrm{d}N. \tag{13.5}$$

Also,

$$D = g^{-1}(E/E_0),$$

where g^{-1} is the inverse of g. This allows us to rewrite Eq. (13.5) as

$$(1/E_0)\mathrm{d}E/\mathrm{d}N = g'\left[g^{-1}(E/E_0)\right] f(\Delta\sigma, R, D).$$

The function $g(D)$ can be obtained experimentally by obtaining data in terms of E/E_0 vs. N. We can then evaluate the function f as:

$$f(\Delta\sigma, R, D) = \left(1/g'\left[g^{-1}(E/E_0)\right]\right)(1/E_0)\mathrm{d}E/\mathrm{d}N.$$

We can evaluate the right-hand side of this expression for a range of $\Delta\sigma$, maintaining constant E/E_0, R, etc. If $2S$ is the average crack spacing, then crack density or damage $= 1/2S$. The following relationship was found experimentally for crack growth as a function of cycles, $\mathrm{d}a/\mathrm{d}N$ (Ogin et al. 1985):

$$\mathrm{d}a/\mathrm{d}N \propto \left({\sigma_{\max}}^2 2S\right)^n.$$

Total crack length a is proportional to damage or crack density, D, i.e.,

$$\mathrm{d}D/\mathrm{d}N \propto \left({\sigma_{\max}}^2/D\right)^n.$$

Modulus of the damaged material E is given by

$$E = E_0(1 - cD), \tag{13.6}$$

where c is a material constant.

For a given value of E/E_0, we can write the modulus or stiffness reduction rate as

$$(-1/E_0)\mathrm{d}E/\mathrm{d}N = A\left[{\sigma_{\max}}^2/{E_0}^2(1 - E/E_0)\right]^n, \tag{13.7}$$

where A and n are constants. The left-hand side of this expression can be determined experimentally. Note that both sides are dimensionless quantities. The modulus reduction rate $(-1/E_0)\mathrm{d}E/\mathrm{d}N$, at a given value of E/E_0, is the tangent to the curve shown in Fig. 13.12. This rate of Young's modulus reduction was well described over the range of peak fatigue stress between 110 and 225 MPa for the glass fiber/epoxy composite by Eq. (13.7); see Fig. 13.13. We can integrate Eq. (13.7) to obtain a diagram relating stiffness reduction to number of cycles for different stress levels, as shown in Fig. 13.14. Such a diagram can be a very useful design aid: It gives us the number of cycles it will take, when the composite is cycled at a certain fraction of the monotonic ultimate strength, to attain a specific amount of stiffness reduction (i.e., a specific amount of damage that the component or the structure can withstand.)

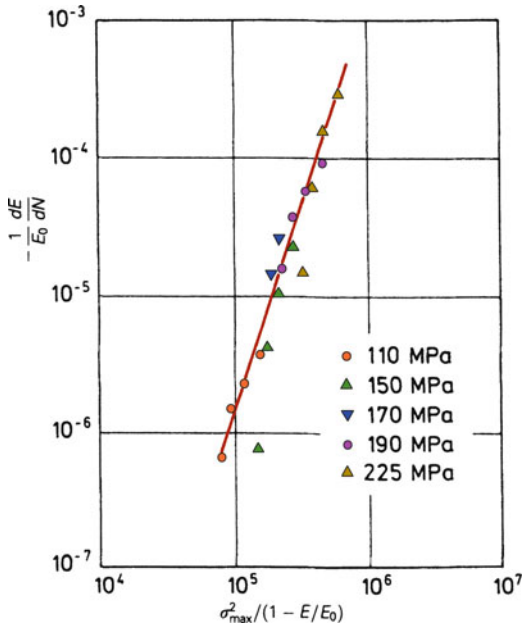

Fig. 13.13 Modulus reduction rate vs. a parameter involving the peak stress [after Ogin et al. (1985)]

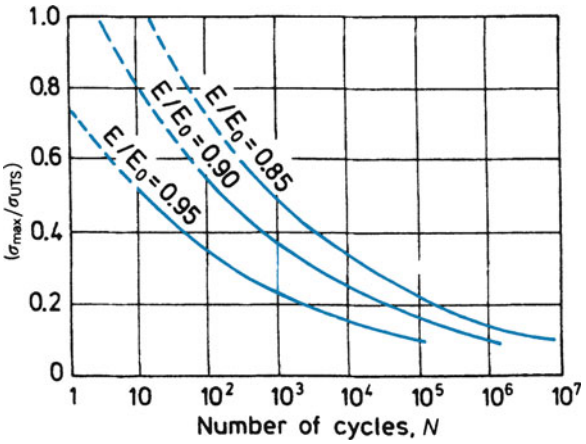

Fig. 13.14 Number of cycles required to attain a given stiffness reduction after cycling at different fractions of the ultimate tensile strength σ_{UTS} [after Ogin et al. (1985)]

13.1.4 Thermal Fatigue

There exists a very fundamental physical incompatibility between the reinforcement (be that fiber, whisker, or particle) and the matrix, to wit, the difference in their thermal expansion (or contraction) coefficients. This problem of thermal expansion mismatch between the components of a composite is a very important one. Thermal stresses arise in composite materials due to the generally large differences in the thermal expansion coefficients (α) of the fiber and the matrix. It should be emphasized that thermal stresses in composites cannot be alleviated by slow cooling or some kind of annealing treatment, techniques that might work in conventional material. The reason for this is that the thermal mismatch will be there even if the temperature change is uniform throughout the volume of the composite. Thermal stresses can be introduced in composites during cooling from high temperature of fabrication, annealing, or curing temperatures or during any temperature excursions (inadvertent or by design) during service. Turbine blades, for example, are very much susceptible to thermal fatigue. The magnitude of thermal stresses in composites is proportional to $\Delta\alpha\Delta T$, where $\Delta\alpha$ is the difference in the expansion coefficients of the two components and ΔT is the amplitude of the thermal cycle (see Chap. 10).

In PMCs and MMCs, the matrix generally has a much higher coefficient of thermal expansion than the fiber. In CMCs, the thermal coefficients of the components may not be that much different but the ceramic materials have very low strain-to-failure values, i.e., very low ductility. In general, the matrix has a much higher coefficient of thermal expansion than the fiber. Rather large internal stresses can result when fiber reinforced composites are heated or cooled through a temperature range. When this happens in a repeated manner, we have the phenomenon of *thermal fatigue*, because the cyclic stress is thermal in origin.

Thermal fatigue can cause cracking in the brittle polymeric matrix or plastic deformation in a ductile metallic matrix (Chawla 1973a, b, 1975a, b). Cavitation in the matrix and fiber/matrix debonding are other forms of damage observed due to thermal fatigue in composites (Chawla 1973a, b, 1975b; Lee and Chawla 1987; Lee et al. 1988). Xu et al. (1995) studied the damage evolution as a function of thermal cycles in terms of three metal matrix systems: Al_2O_{3f}/Mg alloy, B_4C_p/6061 A1 alloy, and SiC_p/8090 A1 alloy. The samples were thermally cycled between room temperature (22 °C) and 300 °C. The incidence of void formation at the fiber/matrix interface increased with the number of cycles. They observed that loss in stiffness and density could be used as damage parameters. The damage in density and elastic modulus caused by thermal cycling was more severe in the fiber reinforced composite than in the particle reinforced composites.

There has been some work involving the use of X-ray tomography to characterize the internal damage in the form of cavitation in particle reinforced MMCs. This is a very impressive tool, although it must be recognized that such equipment is not a common item, i.e., one has to go to some large scale facility, but it would appear that the effort is worth it. Figure 13.15a show the surface of SiC_p/Al composite after thermal cycling. No damage is visible. However, when examined by X-ray tomography, we observe the damage in the interior of the same sample; see Fig. 13.15b.

In view of the fact that CMCs are likely to find major applications at high temperatures, it is of interest to study their behavior under conditions of isothermal exposure as well as under conditions of thermal cycling. Wetherhold and Zawada (1991) studied the behavior of ceramic-grade Nicalon fiber in an aluminosilicate glass matrix under isothermal and thermal cycling conditions. At 650–700 °C, isothermally exposed and thermally cycled samples showed rapid oxidation and loss in strength. Oxidation behavior overshadowed any thermal cycling effect for these test conditions. The embrittlement was attributed to oxygen infiltration from the surface, which destroyed the weak carbon-rich interface in this composite. At 800 °C, however, less embrittlement was observed and the fiber toughening effect remained. This decreased embrittlement at higher temperatures was attributed to smoothening of the sample surface by glass flow and slow oxygen infiltration. Boccaccini et al. (1997, 1998) studied the cyclic thermal shock behavior of Nicalon fiber reinforced glass matrix composites. The thermal mismatch between the fiber and the matrix in this system was almost nil. A decrease in Young's modulus and a simultaneous increase in internal friction as a function of thermal cycles were observed. The magnitude of internal friction was more sensitive to microstructural damage than Young's modulus. An interesting finding of theirs involved the phenomenon of crack healing when the glass matrix composite was cycled to a temperature above the glass transition temperature of the matrix where the glass flowed and caused crack healing.

It is possible to obtain a measure of the internal stresses generated on subjecting a composite to thermal cycling. Kwei and Chawla (1992) used a computer-controlled servohydraulic thermal fatigue system to perform tests on an alumina fiber/AlLi alloy composite. Thermal fatigue testing in this case involved subjecting

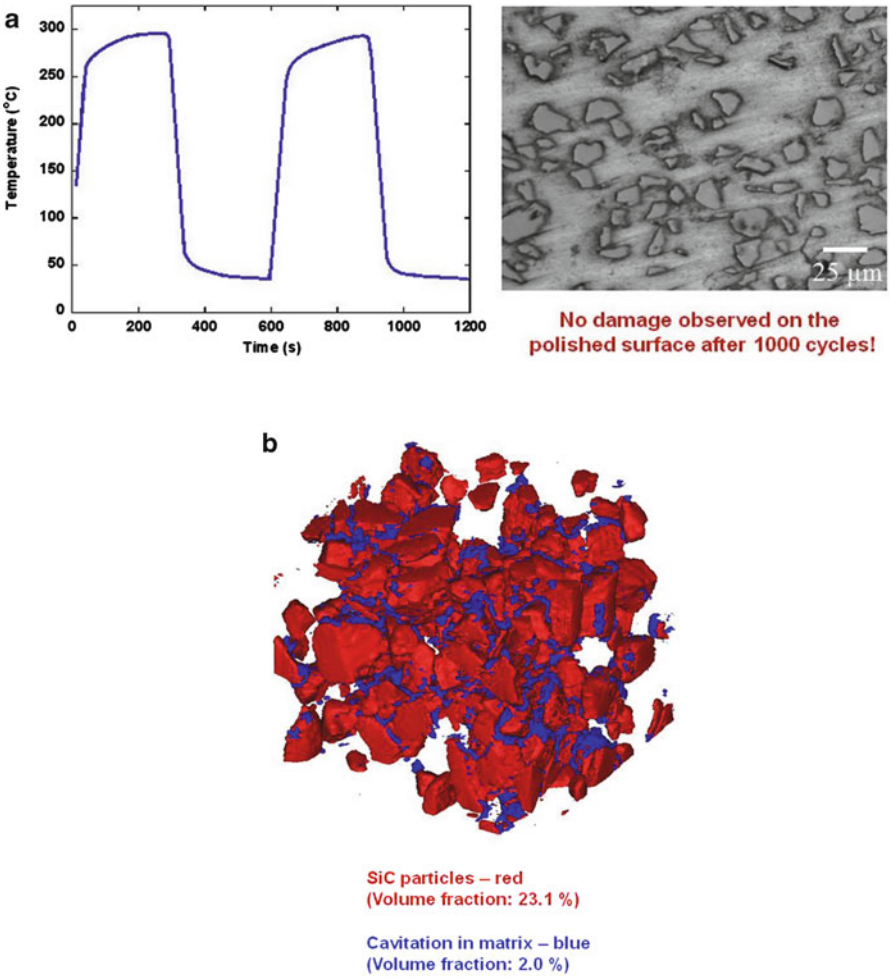

Fig. 13.15 (**a**) Surface of SiC_p/Al composite after thermal cycling. No damage is visible on the surface. (**b**) Same sample examined by X-ray tomography shows damage in the interior. *Blue* color shows cavitation, about 2 % by volume. The SiC particles are about 25–30 μm in diameter and 20 vol.% [courtesy of N.C. Chapman and N. Chawla, Arizona State University]

the sample to thermal cycling while its gage length of the sample was kept constant. This constraint resulted in a stress on the sample, which was measured. Such a test provides the stress required to keep the specimen gage length constant as a function of thermal cycles i.e., a measure of internal stresses generated.

In general, one can reduce the damage in the matrix by choosing a matrix material that has a high yield strength and a large strain to failure (i.e., ductility). The eventual fiber/matrix debonding can only be avoided by choosing the components such that the difference in the thermal expansion characteristics of the fiber and the matrix is low.

13.2 Creep

Creep is defined as the time-dependent deformation in a material. It becomes important at relatively high temperatures, especially at temperatures greater than 0.4–0.5T_H, where T_H is the homologous temperature equal to T/T_m, T is the temperature of interest in kelvin, and T_m is the melting point of the material in kelvin. The phenomenon of creep can cause small deformations under a sustained load over a long period of time. In a variety of situations or equipments (e.g., a pressure vessel or a rotating component), such slow deformations can lead to dimensional problems or even failure. Creep sets a limit on the maximum service temperature. In general, this limit increases with the melting point of a material. Without going into the theoretical and modeling details, suffice it to say that the basic governing equation of creep can be written in the following form:

$$\dot{\varepsilon} = A(\sigma/G)^n \exp(-\Delta Q/kT),$$

where $\dot{\varepsilon}$ is the creep strain rate, σ is the applied stress, n is an exponent, G is the shear modulus, ΔQ is the activation energy for creep, k is the Boltzmann's constant, and T is the temperature in kelvin. The stress exponent, n, typically varies between 3 and 7 in the dislocation climb regime and between 1 and 2 when diffusional mechanisms are operating. Pure dislocation creep, grain boundary sliding, vacancy motion in grains and in the grain boundaries can cause creep. The applied stress, grain size, porosity, and impurity content are important variables.

In polymers and PMCs such as Kevlar 49 aramid fiber/epoxy, one can observe creep even at room temperature (Eriksen 1976). At a given temperature, cross-linked thermosets show less creep than thermoplastics. Creep in polymers is the same as defined above, viz., we apply a constant stress and observe the strain as a function of time. There is a related phenomenon called *stress relaxation*, which is also important in polymers. In stress relaxation, we impose a constant strain on the specimen and observe the drop in stress as a function of time. If we substitute a polymeric fiber such as aramid with a more creep-resistant fiber—say alumina, SiC, or even glass—we can make the composite more creep-resistant.

In very simple terms, creep in a PMC or MMC is likely to be dominated by the creep behavior of the matrix. As the matrix deforms in creep, the applied load is transferred to the load-bearing component, viz., fiber. Eventually, the fibers will carry all the load. McLean (1983, 1985) showed that for a composite containing a matrix that follows a power-law creep ($\dot{\varepsilon} = A\sigma^n$), the creep rate in the composite is given by:

$$\dot{\varepsilon}_c = \frac{A\sigma^n \left[1 - \dfrac{\dot{\varepsilon}}{\dot{\varepsilon}_\infty}\right]^n}{\left[1 + \dfrac{V_f E_f}{V_m E_m}\right] V_m^n},$$

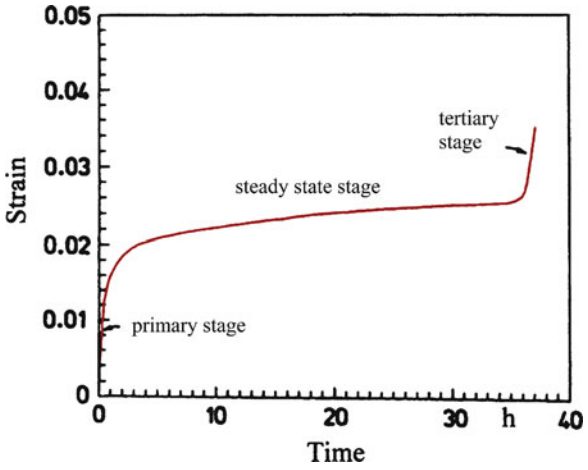

Fig. 13.16 A creep curve, strain vs. time, for a 25 % V_f silicon carbide whisker/2124 aluminum alloy matrix [after Lilholt and Taya (1987)]

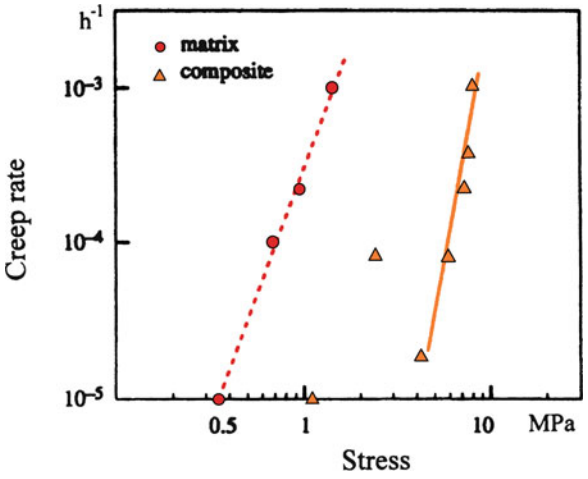

Fig. 13.17 The steady-state creep rate as a function of applied stress for the unreinforced silver matrix and tungsten fiber/silver matrix composite at 600 °C [after Kelly and Tyson (1966)]

where $\dot{\varepsilon}_\infty = (\sigma_c / V_f E_f)$ is the asymptotic creep strain.

A creep curve, strain vs. time, for a 25 % V_f silicon carbide whisker/2124 aluminum alloy matrix is shown in Fig. 13.16 (Lilholt and Taya 1987). The primary, secondary or steady-state, and tertiary stages are indicated. The steady-state creep rate as a function of applied stress for the unreinforced silver matrix and tungsten fiber/silver matrix composite at 600 °C are shown in Fig. 13.17 (Kelly and Tyson 1966). The minimum creep rate as a function of the applied stress for Saffil short fiber reinforced aluminum alloys and unreinforced aluminum alloys is shown in Fig. 13.18 (Dlouhy et al. 1993). Note that the creep rate for the composite is lower than that of the control alloy, but the stress exponent or slope of the composite is much higher than that of the unreinforced alloy.

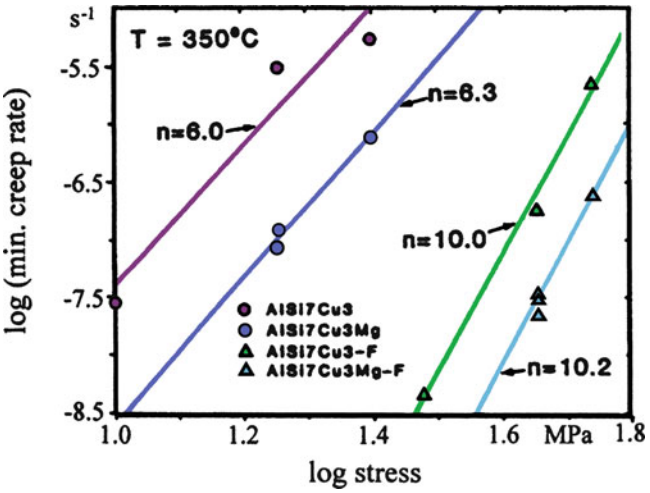

Fig. 13.18 The minimum creep rate as a function of the applied stress for Saffil short fiber reinforced aluminum alloys and unreinforced aluminum alloys. Note that the creep rate for the composite is lower than that of the control alloy, but the stress exponent or slope of the composite is much higher than that of the unreinforced alloy [after Dlouhy et al. 1993]

The anomalously high values of the stress exponent, n, and activation energy, Q, have been explained by using the concept of a threshold stress (Webster 1982; Nieh 1984; Nardone and Strife 1987). Nardone and Strife (1987) used the concept of a threshold stress σ_R, for creep deformation in composites. This theory was originally used to explain the high values for Q and n in dispersion-strengthened alloys (Davies et al. 1973; Parker and Wilshire 1975; Nardone and Tien 1986; Kerr and Chawla 2004). By introducing the threshold stress, the general steady-state creep rate is modified to:

$$\dot{\varepsilon}_{ss} = A\left(\frac{\sigma - \sigma_R}{E}\right)^n \exp\left(\frac{-Q}{RT}\right),$$

where A is a constant, E is the elastic modulus of the composite, and Q is the activation energy. The threshold stress in the discontinuously reinforced composite system can be attributed to a variety of sources (Dunand and Derby 1993; Pandey et al. 1992): (1) Orowan bowing between particles, (2) back-stress associated with dislocation climb, (3) attractive force between dislocations and particles, resulting from relaxation of the strain field of dislocations at the particle/matrix interface (Artz and Wilkinson 1986).

A threshold stress approach cannot always be used to explain the higher stress exponents observed in MMCs, when compared to the unreinforced alloy. Load transfer to the reinforcement, despite the lower aspect ratios of particles and whiskers, is significant, as the applied load is carried by the high stiffness reinforcement. With increasing load transfer to the reinforcement, the resolved shear stress

on dislocations in the matrix may be lowered significantly below that required for Orowan bowing. Dragone and Nix (1992) studied the creep behavior of Al_2O_3 short fiber reinforced Al–5 % Mg alloy between 200 and 400 °C. They also observed anomalously high values of stress exponent ($n \sim 12$–15) in the composites, while the unreinforced alloy exhibited much lower, typical values ($n \sim 3$). The measured activation energy (225 kJ/mol) for the composites was also anomalously high. A threshold stress analysis showed that the contribution from Orowan bowing was very small. Using a model consisting of randomly oriented short fibers in the Al alloy matrix, and considering the progressive damage to the fibers during creep, they were able to predict the experimentally observed high values of stress exponent and activation energy. Dragone and Nix (1992) also noted that the arrangement of fibers has a significant effect on the degree of matrix constraint. A decrease in effective stress (increase in matrix constraint) was observed with increasing volume fraction, fiber aspect ratio, and degree of overlap between fibers. The normal and shear stresses at the fiber/matrix interface were also quite large, indicating that void growth or debonding might take place during the creep process.

In some cases, creep behavior of MMCs shows a close correlation between the properties of the matrix and those of the composite (Kelly and Tyson 1966; Kelly and Street 1972a, b; Dragone et al. 1991). In other cases, this is not observed. Creep experiments on an aluminum matrix containing ceramic particles or short fibers show a very high value of stress exponent, $n \sim 20$ and an activation energy for creep, $Q \sim 225$–400 kJ/mol. This is in contrast to the activation energy for self-diffusion in aluminum matrix, $Q \sim 150$ kJ/mol (Nieh 1984; Nardone and Strife 1987; Morimoto et al. 1988; Pandey et al. 1992; Dragone and Nix 1992; Dlouhy et al. 1993; Eggeler and Dlouhy 1994). Various models have been proposed to rationalize these discrepancies. For a review of these models, the reader is referred to a review article by Dunand and Derby (1993).

In CMCs too, the incorporation of fibers or whiskers can result in improved creep resistance. The creep rate, in four-point bending, of silicon carbide whisker (20 v/o)-reinforced alumina was significantly reduced compared to that of the unreinforced alumina (Lin and Becher 1990). For the creep tests done at 1,200 and 1,300 °C, the stress exponent, n in the expression $\dot{\varepsilon} = A(\sigma)^n$, was 2 for the composite, not much different from the value of 2.3 for the unreinforced alumina, indicating that the creep rate controlling process was similar in these two materials at these two temperatures. This improvement was attributed to a retardation of grain boundary sliding by SiC whiskers present at the grain boundaries. The creep curve at 1,400 °C for the composites showed a marked change in the n value at a stress level of about 125 MPa indicating a change in the rate controlling process. A stress exponent value of about 2 is generally thought to be due to grain boundary sliding. The higher stress exponent and the higher creep rate at 1,400 °C was attributed by the authors to extensive cavitation. There are, however, some differences in the creep behavior of CMCs vis-à-vis MMCs. Wiederhorn and Hockey (1991) have analyzed the creep behavior of CMCs, both particle and whisker reinforced. In two-phase ceramics, creep rate in tension was faster than in compression for identical stress and temperature conditions. At first sight, this might appear to be due to the ease of cavitation and microcracking during tension rather than in compression

because tensile stresses assist cavitation while compressive stresses tend to close the cavities and micro-cracks. This is not so because Wiederhorn et al. (1988) observed the asymmetry in creep behavior in CMCs even under conditions where cavitation was absent.

Although continuous ceramic fibers can lead to substantial toughening of ceramics at room temperature, most of these fibers are not sufficiently creep-resistant. In fact, creep rates of many fibers are much higher than those of the corresponding monolithic ceramics (Lin and Becher 1990; Routbort et al. 1990; Bender et al. 1991; Pysher et al. 1989). In the case of creep of ceramic matrix composites, one needs to consider the intrinsic creep resistance of the fiber, matrix, and interface region. Oxide fibers are fine-grained and generally contain some glassy phase. Nonoxide fibers are also fine-grained, multiphasic (with some glassy phase), and susceptible to oxidation (Bender et al. 1991). Nonoxide fiber/nonoxide matrix composites, such as SiC/SiC and SiC/Si_3N_4, generally show good low-temperature strength, but their poor oxidation resistance is a major limitation. Mah et al. (1984) observed that the strength of Nicalon-type SiC fiber was very sensitive to temperature above 1,200 °C and its environment. Nonoxide fiber/oxide matrix composites or oxide fiber/nonoxide matrix composites, such as carbon/glass, SiC/glass, SiC/alumina, and Al_2O_3/SiC, generally do not possess high oxidation resistance because the permeability constant for the diffusion of oxygen is high, resulting in rapid oxygen permeation through the oxide matrix. Prewo et al. (1986) found that the glass matrix did not prevent the degradation of carbon fiber caused by oxidation. Holmes (1991) observed the formation of a complex glass layer (SiO_2–Y_2O_3–MgO) on the surface of hot-pressed SCS-6/Si_3N_4 subjected to creep. The glass layer forms by oxidation of silicon nitride and sintering aids. He also observed that the extent of fiber pullout decreased as the applied stress increased in a creep test. Rather pronounced separation along the fiber/matrix interface was observed after low stress (70 MPa) creep.

Creep behavior of laminated ceramic composites has also been studied. The steady-state creep rate of monolithic silicon nitride matrix, [0] and [0/90] cross-plied SCS-6/Si_3N_4 composites as a function of applied stress at 1,200 °C showed that the creep resistance of the composite was superior to that of the monolithic silicon nitride, while the creep resistance of the unidirectional composite was superior to that of the cross-plied composite because the fibers in the 90° direction contribute less to creep resistance than the fibers in the 0° direction (Yang and Chen 1992).

From the preceding discussion of high-temperature behavior of nonoxide composites (even when one component is a nonoxide), it would appear that in situations where stability in air at high temperatures is a prime objective, oxide fiber/oxide matrix composites should be most promising because of their inherent stability in air. Some such systems have been investigated (Chawla et al. 1996a, b). Among the oxide fibers, alumina-based and mullite fibers are the most widely used, while glass, glass–ceramics, alumina, and mullite are the most widely used oxide matrices. One can have two categories of oxide/oxide composites: oxide matrix reinforced with uncoated oxide fibers and oxide matrix reinforced with coated oxide fibers. In the first category of oxide/oxide composites, strength and modulus

of the composite are generally better than the unreinforced oxide. The toughness characteristics of these composites are not substantially changed because of the strong chemical bonding at the fiber/matrix interface. Interface tailoring via fiber coating (the second category) is employed extensively in order to achieve the desired properties of the composites.

13.3 Closure

Let us summarize the important points of this chapter. In general, the fatigue resistance of a given material can be enhanced by reinforcing it with continuous fibers or by bonding two different metals judiciously selected to give the desired characteristics. Not unexpectedly, the improvement is greatest when the fibers are aligned parallel to the stress direction. While conventional approaches such as stress vs. cycles (S–N) curves or fatigue crack propagation tests under conditions of self-similar crack propagation can be useful for comparative purposes and for obtaining information on the operative failure mechanisms, they do not provide information useful to designers. Fatigue crack propagation under mixed-mode cracking conditions should be analyzed analytically and experimentally. Novel approaches such as that epitomized by the measurement of stiffness reduction of the composite as a function of cycles seem to be quite promising. Because many applications of composites do involve temperature changes, it is important that thermal fatigue characteristics of these composites be evaluated in addition to their mechanical fatigue characteristics.

In regard to creep behavior of composites, introduction of creep-resistant reinforcement, especially fibers in a matrix that undergoes substantial creep, can result in a composite that is more creep-resistant than the unreinforced matrix. Experimental observations show that the stress exponent for the composite in the creep rate vs. stress curve is frequently much higher than that for the unreinforced alloy.

References

Allison JE, Jones JW (1993) In: Suresh S, Mortensen A, Needleman A (eds) Fundamentals of metal matrix composites. Butterworth-Heinemann, Boston, MA, p 269

Artz E, Wilkinson DS (1986) Acta Metall 34:1893

Beaumont PWR (1989) In: Phillips LN (ed) Design with advanced composite materials. Springer, Berlin, p 303

Bender BA, Wallace JS, Schrodt DJ (1991) J Mater Sci 12:970

Boccaccini AR, Pearce DH, Janczak J, Beier W, Ponton CB (1997) Mater Sci Technol 13:852

Boccaccini AR, Ponton CB, Chawla KK (1998) Mater Sci Eng A241:142

Bonnen JJ, You CP, Allison JE, Jones JW (1990) Proc Int Conf Fatigue. Pergamon, New York, p 887

Champion AR, Krueger WH, Hartman HS, Dhingra AK (1978) Proc:1978 Intl Conf Compos Mater (ICCM/2). TMS-AIME, New York, p 883

Chawla KK (1973a) Metallography 6:155
Chawla KK (1973b) Philos Mag 28:401
Chawla KK (1975a) Fibre Sci Technol 8:49
Chawla KK (1975b) In: Grain boundaries in eng. materials, Proc. 4th Bolton landing conf. Claitor's Pub. Div., Baton Rouge, LA, p 435
Chawla KK, Liaw PK (1979) J Mater Sci 14:2143
Chawla KK, Schneider H, Xu ZR, Schmücker M (1996) In: High temperature materials: design & processing considerations, Engineering foundation conference, Davos, Switzerland, TMS, Warrendale, PA, 19–24 May. p 235
Chawla N (1997) Met Mater Trans 28A:2423
Chawla N, Holmes JW, Lowden RA (1996b) Scripta Mater 35:1411
Chawla N, Andres C, Jones JW, Allison JE (1998a) Metall Mater Trans 29:2843
Chawla N, Tur YK, Holmes JW, Barber JR, Szweda A (1998b) J Am Ceram Soc 81:1221
Chawla N, Kerr M, Chawla KK (2005) J Am Ceram Soc 88:101
Chawla N, Ganesh VV (2010) Int J Fatigue 32:856
Christman T, Suresh S (1988a) Acta Metall 36:1691
Christman T, Suresh S (1988b) Mater Sci Eng 102A:211
Crowe CR, Hasson DF (1982) In: Proc. 6th Int Conf. on the strength of metals and alloys. Pergamon, Oxford, p 859
Davidson DL (1989) Eng Fract Mech 33:965
Davies PW, Nelmes G, Williams KR, Wilshire B (1973) Metal Sci J 7:87
Dlouhy A, Merk N, Eggeler G (1993) Acta Metall Mater 41:3245
Dragone TL, Nix WD (1992) Acta Metall Mater 40:2781
Dragone TL, Schlautmann JJ, Nix WD (1991) Metall Trans 22A:1029
Dunand DC, Derby B (1993) In: Suresh S, Mortensen A, Needleman A (eds) Fundamentals of metal matrix composites. Butterworth-Heinemann, Boston, MA, p 191
Dvorak GJ, Johnson WS (1980) Int J Fracture 16:585
Eggeler G, Dlouhy A (1994) In: Chawla KK, Liaw PK, Fishman SG (eds) High performance composites: commonalty of phenomena. TMS, Warrendale, PA, p 477
Eriksen RH (1976) Composites 7:189
Godefroid LB, Chawla KK (1988) In: 3rd Latin American colloquium on fatigue and fracture of materials, Rio de Janeiro, Brazil
Goel A, Chawla KK, Vaidya UK, Chawla N, Koopman M (2009) Mater Charact 60:537
Gomez JP, Wawner FW (1988) Personal communication
Gouda M, Prewo KM, McEvily AJ (1981) In: Fatigue of fibrous composite materials, ASTM STP 723. American Society of Testing and Materials, Philadelphia, PA, p 101
Hack JE, Page RA, Leverant GR (1987) Met Trans A 15A:1389
Hahn HT, Kim RY (1976) J Compos Mater 10:156
Hahn HT, Lorenzo L (1984) In: Advances in fracture research, ICF6, Vol. 1. Pergamon, Oxford, p 549
Han LX, Suresh S (1989) J Am Ceram Soc 72:1233
Helms HE, Haley PJ (1989) In: Tennery VJ (ed) Ceramic materials and components for engines. Amer. Ceram. Soc, Westerville, OH, p 1347
Highsmith AL, Reifsnider KL (1982) In: Damage in composite materials, ASTM STP 775. Amer. Soc. of Testing and Mater, Philadelphia, PA, p 103
Holmes JW (1991) J Mater Sci 26:1808
Izuka Y, Norita T, Nishimura T, Fujisawa K (1986) In: Carbon fibers. Noyes Pub, Park Ridge, NJ, p 14
Johnson WS (1988) In: *Mechanical and Physical Behavior of Metallic and Ceramic Composites*, 9th Risø Intl. Symp. on Metallurgy and Materials Science, Riso Nat. Lab., Roskilde, Denmark, p 403
Johnson WS, Wallis RR (1986) Composite materials: fatigue and fracture, ASTM STP 907. ASTM, Philadelphia, PA, p 161
Karandikar PG, Chou T-W (1992) Ceram Eng Sci Proc 13:882

Kelly A, Street KN (1972a) Proc R Soc Lond A 328:267
Kelly A, Street KN (1972b) Proc R Soc Lond A 328:283
Kelly A, Tyson WR (1966) J Mech Phys Solids 14:177
Kerr M, Chawla N (2004) Acta Mater 52:4527
Kumai S, Knott JF (1991) Mater Sci Eng A146:317
Kumai S, King JE, Knott JF (1990) Fatigue Fract Eng Mater Struct 13:511
Kwei LK, Chawla KK (1992) J Mater Sci 27:1101
Lavengood RE, Gulbransen LE (1969) Polym Eng Sci 9:365
Lee CS, Chawla KK (1987) In: Proc.: Industry-University Adv. Mater. Conf. TMS-AIME, Warrendale, PA, p 289
Lee CS, Chawla KK, Rigsbee JM, Pfeifer M (1988) In: Cast reinforced metal composites. ASM Int, Metals Park, OH, p 301
Levin M, Karlsson B, Wasén J (1989) In: Fundamental relationships between microstructures and mechanical properties of metal matrix composites. TMS, Warrendale, PA, p 421
Lilholt H, Taya M (1987) Proc: ICCM/6. Elsevier, Barking, pp 2.234–2.244
Lin H-T, Becher PF (1990) J Am Ceram Soc 73:1378
Logsdon WA, Liaw PK (1986) Eng Fract Mech 24:737
Mah T, Hecht NL, McCullum DE, Hoenigman JR, Kim HM, Katz AP, Lipsitt HA (1984) J Mater Sci 19:1191
Mandell JF, Mcgarry FJ, Huang DD, Li CG (1983) Polym Compos 4:32
McCartney RF, Richard RC, Trozzo PS (1967) Trans ASM 60:384
McGuire MA, Harris B (1974) J Phys D Appl Phys 7:1788
McLean M (1983) Directionally solidified materials for high temperature service. The Metals Soc, London
McLean M (1985) Proc.: 5th Intl. Conf. on Composite Materials (ICCM/V). TMS-AIME, Warrendale, PA, p 639
Morimoto T, Yamaoka T, Lilholt H, Taya M (1988) J Eng Mater Tech Trans ASME 110:70
Nardone VC, Strife JR (1987) Metall Trans 18A:109
Nardone VC, Tien JK (1986) Scripta Mater 20:797
Nieh TG (1984) Metall Trans 15A:139
O'Brien TK (1984) Interlaminar fracture of composites. NASA TM 85768
O'Brien TK, Reifsnider KL (1981) J Compos Mater 15:55
Ogin SL, Smith PA, Beaumont PWR (1985) Compos Sci Technol 22:23
Owens MJ, Dukes R (1967) J Strain Anal 2:272
Owens MJ, Smith TR, Dukes R (1969) Plast Polymers 37:227
Page RA, Hack JE, Sherman R, Leverant GR (1987) Met Trans A 15A:1397
Pandey AB, Mishra RS, Mahajan YR (1992) Acta Metall Mater 40:2045
Paris PC, Erdogan F (1963) J Basic Eng Trans ASME 85:528
Parker JD, Wilshire B (1975) Metal Sci J 9:248
Pfeiffer NJ, Alic JA (1978) J Eng Mater Technol 100:32
Phillips DC (1983) In: Handbook of composites, vol 4. North-Holland, Amsterdam, p 472
Prewo KM, Brennan JJ, Layden GK (1986) Am Ceram Soc Bull 65:305
Pruitt L, Suresh S (1992) J Mater Sci Lett 11:1356
Pysher DJ, Goretta KC, Hodder RS Jr, Tressler RE (1989) J Am Ceram Soc 72:284
Ramakrishnan V, Jayaraman N (1993) J Mater Sci 28:5580
Reifsnider KL, Henneke EG, Stinchcomb WW, Duke JC (1981) In: Mechanics of Composite materials. Pergamon, New York, p 399
Rohatgi PK, Asthana R, Tewari SN, Narendranath CS (1994) In: Chawla KK, Liaw PK, Fishman SG (eds) High performance composites: commonalty of phenomena. TMS, Warrendale, PA, p 93
Routbort JL, Goretta KC, Dominguez-Rodriguez A, de Arrellano-Lopez AR (1990) J Hard Mater 1:221
Saff CR, Harmon DM, Johnson WS (1988) J Met 40:58
Shang JK, Yu W, Ritchie RO (1988) Mater Sci Eng A102:181

Sørensen BF, Holmes JW (1995) Scripta Met Mater 32:1393
Stoloff NS (1987) Advances in composite materials. Applied Sci. Pub, London, p 247
Suresh S (1991) J Hard Mater 2:29
Suresh S, Han LX, Petrovic JJ (1988) J Am Ceram Soc 71:l58–161
Talreja R (1985a) Fatigue of composite materials. Technical University of Denmark, Lyngby
Taylor LG, Ryder DA (1976) Composites 1:27
Wang Z, Laird C, Hashin Z, Rosen BW, Yen CF (1991) J Mater Sci 26:5335
Webster D (1982) Metall Mater Trans 13A:1511
Wetherhold RC, Zawada LP (1991) In: Fractography of glasses and ceramics. In: Frechete VD, Varner JR (eds) Ceramic transactions, vol 17. Amer. Ceram. Soc, Westerville, OH, p 391
Wiederhorn SM, Hockey BJ (1991) Ceram Int 17:243
Wiederhorn SM, Liu W, Carroll DF, Chuang T-J (1988) J Am Ceram Soc 12:602
Williams DR, Fine ME (1985) In: Proc.: Fifth Intl Conf. Composite Materials (ICCM/V). TMS-AIME, Warrendale, PA, p 639
Williams DR, Fine ME (1987) In: Proc.: 6th Intl. Conf. on Composite Materials (ICCM/VI), vol 2. Elsevier Applied Science, London, p 113
Xu ZR, Chawla KK, Wolfenden A, Neuman A, Liggett GM, Chawla N (1995) Mater Sci Eng A A203:75
Yang J-M, Chen ST (1992) Adv Compos Lett 1:27

Further Reading

Hertzberg RW, Manson JA (1980) Fatigue of engineering plastics. Academic, New York
Talreja R (1985b) Fatigue of composite materials. Technical University of Denmark, Lyngby
Talreja R (ed) (1994) Damage mechanics of composite materials. Elsevier, Amsterdam

Problems

13.1. List some of the possible fatigue crack initiating sites in particle, short fiber, and continuous fiber reinforced composites.

13.2. What factors do you think will be important in the environmental effects on the fatigue behavior of fiber reinforced composites?

13.3. Acoustic emission can be used to monitor damage in carbon fiber/epoxy during fatigue. Under steady loading conditions the damage is controlled by fiber failure and one can describe the acoustic emission by

$$\frac{\mathrm{d}N}{\mathrm{d}t} = \frac{A}{(t+T)^n}$$

where N is the total number of emissions, t is the time, T is a time constant, and A is constant under steady loading conditions. Taking $n = 1$, show that log t is a linear function of the accumulated counts (Hint: see Fuwa M, Harris B, Bunsell AR (1975) J Appl Phys 8: 1460).

13.4. Discuss the effects of frequency of cycling in regard to hysteretic heating in PMCs and CMCs.
13.5. Discuss the fatigue behavior an aramid fiber reinforced PMC is subjected to fatigue at negative and positive stress ratio (R).
13.6. Which one will have a better creep resistance in air: an oxide/oxide composite or a nonoxide/nonoxide system? Explain your answer.
13.7. Diffusional creep involving mass transport becomes important at low stresses and high temperatures. Discuss the importance of reinforcement/matrix interface in creep of a composite under these conditions.
13.8. Assume that the creep of fiber and matrix can be described by a power-law and that a well bonded interface exists. Assume also that the strain rate of the composite is given be the volume weighted average of the strain rates of the fiber and matrix. Derive an expression for the strength of such a composite.
13.9. In some composites, residual thermal stress distribution obtained at room temperature on cooling from the high processing temperature results in compressive radial gripping at the interface. Discuss the effect of high temperatures or creep in such a composite.